Journal Pre-proof

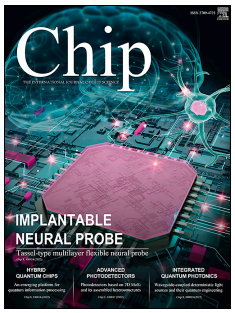


# Travelling-wave Parametric Amplifier Induced Qubit Dephasing: Analysis and Mitigation

Yingshan Zhang, Huikai Xu, Yu Song, Yuqun Xu, Shuang Yang, Ziyue Hua, Shoukuan Zhao, Weiyang Liu, Guangming Xue, Yirong Jin, Haifeng Yu

PII: S2709-4723(23)00030-8

DOI: https://doi.org/10.1016/j.chip.2023.100067

Reference: CHIP 100067

To appear in: *Chip*

Received Date: 12 May 2023

Revised Date: 24 August 2023

Accepted Date: 5 September 2023

Please cite this article as: Zhang Y, Xu H, Song Y, Xu Y, Yang S, Hua Z, Zhao S, Liu W, Xue G, Jin Y, Yu H, Travelling-wave Parametric Amplifier Induced Qubit Dephasing: Analysis and Mitigation, *Chip*, https://doi.org/10.1016/j.chip.2023.100067.

# Travelling-wave Parametric Amplifier Induced Qubit Dephasing: Analysis and Mitigation

Yingshan Zhang[a], Huikai Xu[a], Yu Song[a], Yuqun Xu[a], Shuang Yang[a], Ziyue Hua[b], Shoukuan Zhao[a], Weiyang Liu[a,*], Guangming Xue[a,**], Yirong Jin[a], Haifeng Yu[a,c]

[a] *Beijing Academy of Quantum Information Sciences, Beijing, 100193, China*
[b] *Center for Quantum Information, Institute for Interdisciplinary Information Sciences, Tsinghua University, Beijing, 100084, China*
[c] *Hefei National Laboratory, Hefei, 230088, China*

**Abstract**

The mitigation of dephasing poses a significant challenge in improving the performance of error-prone superconducting quantum computing systems. Here, we investigate the dephasing of a transmon qubit in a dispersive readout regime using a Josephson travelling-wave parametric amplifier as the preamplifier. Our findings reveal that the potent pump leakage from the preamplifier may lead to severe dephasing. This issue could be attributed to a mixture of measurement-induced dephasing, ac Stark effect, and heating. We show that pulse-mode readout is a promising measurement scheme to mitigate qubit dephasing while minimizing the need for bulky circulators. Our work provides key insights into mitigating decoherence from microwave-pumped preamplifiers, which will be critical for advancing large-scale quantum computers.

*Keywords:* TWPA, microwave pump, dephasing, pulse mode
*PACS:* 03.65.Yz, 42.50.Dv, 85.25.Am

## 1. INTRODUCTION

Dephasing is a limiting factor in implementing high-fidelity gates on superconducting qubits. Microwave-pumped preamplifiers enable low-noise

*Email: liuwy@baqis.ac.cn(Weiyang Liu)
**Email: xuegm@baqis.ac.cn(Guangming Xue)

qubit measurement but they may induce dephasing when the pump is on. In general, these preamplifiers are based on nonlinear wave mixing, converting pump photons into amplified signal photons. Compared with a reflective Josephson parametric amplifier (JPA)[1], a travelling-wave parametric amplifier (TWPA)[2, 3, 4, 5, 6, 7] is a promising preamplifier for scaling up due to its higher bandwidth and larger dynamical range. But the leakage of the microwave pump may pose a severe dephasing challenge for both types of amplifiers. This problem can impede the development of dynamic quantum circuits [8] and quantum error correction[9], which may open up a powerful pool of algorithms of practical quantum advantage[10]. A good understanding of the origins of such dephasing is in need in order to find a solution.

A circulator is a bulky and ferrite device that can separate the input and output signals of reflective amplifiers. Its two-port version, also known as an isolator, can block the output port from leaking to the input. Currently, the most common solution to the dephasing challenge is to insert circulators. However, this approach sacrifices scalability. While a transmissive TWPA does not need a circulator in principle like a reflective JPA does, it may still require circulators when connecting to the qubit chip in reality. Typically, between the qubit chip and the first amplifier, we have 2-3 stages of circulator for reflective JPA and at least one stage of circulator for TWPA (18 dB isolation per stage). Qubit cloaking[11], active cancellation of pump[12] or dual pumps[13] can also mitigate the dephasing problem but are difficult to calibrate. Additionally, novel amplifier types, such as dc-pumped amplifiers[14] and directional amplifiers[15, 16], may circumvent the problem, but they are still in the early stages of development and have performance limitations to overcome.

To systematically understand and address this dephasing challenge, we study the effects of TWPA on qubit dephasing. Thanks to the high-coherence tantalum-based superconducting transmon qubits[17] and home-made TWPAs, we are able to quantitatively explore the dephasing from pump leakage. In Section 2 we briefly introduce qubit dephasing, TWPA, and how they are connected to each other. Particularly, we discuss multiple aspects of TWPA that can cause qubit dephasing, including backward amplification, leakage of the pump, and backward noise. And we describe a metric to compare different readout modes. Then, in Section 3, we experimentally explore some of these dephasing factors and assess a corresponding solution called pulse-mode readout. We measure the above metric to confirm the effectiveness of our approach. Finally, in Section 4, we conclude about the significance

and future directions of our work. The pulse-mode readout approach surmounts the constraints that plagued previous approaches by extending qubit coherence near the limit without the pump, while minimally sacrificing the readout Signal-to-Noise Ratio (SNR).

## 2. Theoretical foundations and experimental considerations

Within this section, we briefly review the dephasing in superconducting qubits and introduce TWPAs. Drawing upon established knowledge, we aim to identify the origins of TWPA-induced dephasing and put forth a modified measurement efficiency metric to evaluate distinct readout modes.

### *2.1. Relevant dephasing parameters and sources*

Qubit dephasing is typically identified by analyzing the Ramsey oscillation curve. We can determine a characteristic decay time, denoted as $T_2^{\mathrm{R}}$, from this curve. However, it is important to note that $T_2^{\mathrm{R}}$ is not the same as the pure dephasing time, which is represented as $T_\phi$. The relationship between these two quantities is described by the equation $\Gamma_\phi + \Gamma_1/2 = \Gamma_2^{\mathrm{R}} = 1/T_2^{\mathrm{R}}$, where $\Gamma_1$ is the qubit relaxation rate, and $\Gamma_\phi = 1/T_\phi$ is the pure dephasing rate. $\Gamma_\phi$ encompasses all dephasing mechanisms except for relaxation.

Within the realm of superconducting qubits, especially transmon qubits, let us now delve into a detailed examination of the sources of dephasing that pique our interest.

Measurement-induced dephasing is a well-known limitation in superconducting qubit readout, arising from the backaction of the measurement pulse[18]. As the photon number in the readout resonator increases during dispersive measurement, so do fluctuations in both photon number and qubit frequency, manifesting itself as dephasing.

The dominant noise that causes measurement-induced dephasing depends on design parameters. When the dispersive coupling is strong, i.e. $\chi \gg \gamma, \kappa$, shot noise dominates[19], where $\chi$ is the dispersive shift, and $\gamma, \kappa$ are the qubit and resonator decay rates. We often tune $\chi \sim \kappa$ to optimize readout fidelity, making thermal and coherent noise more significant.

The effects of thermal and coherent resonator photons on qubit dephasing have been analyzed[20]. For a resonator with frequency $\omega_r - \chi$ ($\omega_r + \chi$) when the qubit is in $|0\rangle$ ($|1\rangle$), the dephasing caused by a coherent drive with

Hamiltonian $H_p = \hbar\epsilon_p(\hat{a}^\dagger \exp(-i\omega_p t) + h.c.)$ in the zero temperature limit is

$$\Gamma_{\phi,\mathrm{dr}} = 2\epsilon_p^2 \frac{\chi^2\kappa}{[(\delta+\chi)^2 + (\kappa/2)^2]\,[(\delta-\chi)^2 + (\kappa/2)^2]}, \tag{1}$$

where $\delta = \omega_r - \omega_p$ is the detuning of the drive.

Also, the qubit frequency $\omega_q$ shifts due to coherent photons in the resonator by:

$$\Delta\omega_q = 2\chi n_r, \tag{2}$$

where $n_r$ is the average number of photons inside the resonator and can be expressed as[13]

$$n_r = \frac{1}{2}\epsilon_p^2 \left[\frac{1}{(\kappa/2)^2 + (\delta+\chi)^2} + \frac{1}{(\kappa/2)^2 + (\delta-\chi)^2}\right]. \tag{3}$$

Measurement-induced dephasing in the weak coupling limit has been explored experimentally[21]. The effects of thermal photons have also been characterized[22], and cavity attenuators proposed as a promising solution[23].

Another process that contributes to dephasing is quasiparticle injection[24]. For a high-power microwave near the bare resonator frequency of the readout resonator, extra photons in the resonator excited by the pump induce an AC voltage across the junction. If this voltage $V_g \geq 2\Delta/e$ surpasses the superconducting gap $\Delta$, where $e$ is the electron charge, it generates quasiparticles by breaking Cooper pairs. Since the frequency of a transmon qubit depends weakly on offset charge, parity switching due to quasiparticle tunneling also causes dephasing.

In our definition, measurement-induced dephasing is confined to $\omega_p$ near the resonator frequency. Outside this range, the term "ac-Stark effect" is used instead to clarify the discussion. Specifically, this effect occurs when an off-resonant drive acts on a qubit, dressing its frequency. The dressed frequency depends on both the frequency and amplitude of the drive. Any fluctuations in the amplitude of this drive will result in corresponding fluctuations in the dressed frequency, which in turn can induce dephasing. Such fluctuations can arise from the amplitude noise of the microwave source[25, 26]. In addition, this drive may excite spurious modes that couple to the qubit and cause dephasing in the same way as measurement-induced dephasing, although the measurement results are never retrieved. An essential parameter characterizing such a drive is $\theta$, where $\tan\theta = 2\chi/\kappa$, which indicates the measurement

strength. When $\chi/\kappa$ is small, $\theta$ can be approximated as $2\chi/\kappa$. The induced dephasing can then be calculated as [21]

$$\Gamma_{\phi,\mathrm{ac}} = \frac{2P}{\hbar\omega_p}\theta^2, \tag{4}$$

where $P$ represents the power of the incident drive in the steady state, and the frequency shift of the qubit is

$$\Delta\omega_q = \frac{P}{\hbar\omega_p}\theta. \tag{5}$$

Thermal effects can also contribute to dephasing, inclusive but not limited to increased substrate loss, critical current fluctuations of the junction[27], the production of thermal photons in the readout resonator, as well as quasiparticle tunneling.

### *2.2. TWPA*

A TWPA is a two-port device that amplifies signals by utilizing the nonlinearity of an array of Josephson junctions, a long wire with kinetic inductance, or other types of nonlinear transmission lines. It operates based on three- or four-wave mixing, where one or two pump photons are downconverted into a signal photon and an idler photon. By imparting energy from a strong pump wave into the signal wave, the TWPA provides exponential gain to the signal as all waves propagate through it with matched phase.

TWPAs are useful for qubit readout because they can achieve near quantum-limited noise, wide bandwidth, and high gain. Their added noise[28, 29] originates from non-superconducting materials and the intrinsic quantum fluctuations of the signal and idler waves[30], with a minimum of 0.5 photons - the standard quantum limit. Above this limit, the dielectric loss of the TWPA substrate is often dominant[31]. With noise near this limit, a TWPA can significantly increase the SNR compared to commercial high electron-mobility transistor (HEMT) amplifiers.

### *2.3. TWPA induced dephasing*

Although TWPAs offer several advantages, they can also inadvertently dephase qubits and degrade its performance.

The backward amplification process is unique to transmissive amplifiers like the TWPA, as the signal inside a reflective amplifier does not have a defined propagation direction. Unavoidable impedance mismatch between components can produce reflected pump, signal, and idler waves, as Figure 1(a) illustrates. Although designed to be 50 Ohm, a small impedance mismatch persists between the TWPA cell array and input-output ports because of fluctuations in junction critical current and structural transitions. Therefore, the signal can reflect off the output port and transmit backward through the array. If the forward pump, backward signal, and idler waves fulfill energy and momentum conservation, backward amplification occurs[32]. However, this is often difficult to achieve.

TWPA also suffers from the mixing of the reflected pump and reflected signal waves. This process resembles forward amplification but with a weaker reflected pump. Thus, backward amplification is also possible given a large enough impedance mismatch, e.g. if the TWPA array wave impedance reaches 150 Ohm[33].

Beyond backward amplification from the forward or reflected pump, the reflected signal wave can also transmit through the array. If isolation is insufficient, this reflected signal will reach the qubit chip, with the potential to drive the resonator. The effects of this reflected signal are comparable to that of pump leakage, which we will discuss subsequently.

As for pump leakage, We consider a typical setup (Figure 1(a)), where the TWPA is connected to the input port of a directional coupler. The pump enters through the coupled port, while the signal from the qubit, after passing through circulators, enters through the transmitted port. As the transmitted and coupled ports are well isolated, direct pump leakage to the qubit is suppressed. However, the pump strongly reflects off the TWPA due to impedance mismatch. This reflected pump from the input port can travel directly to the transmitted port, reaching the qubit. With no circulators, pump leakage is severe. But adding enough circulator stages solves this problem.

Pump leakage gives rise to a multiplicity of effects, including but not limited to the effects we discussed in the previous subsection: measurement-induced dephasing, quasiparticle injection, ac-Stark effect and heating. For four-wave mixing readout, leaked pump photons have frequency close to readout resonator. For both three- and four-wave mixing, reflected signal photons have the frequency of readout resonator. Both can cause measurement-induced dephasing. When the pump frequency is near the bare resonator

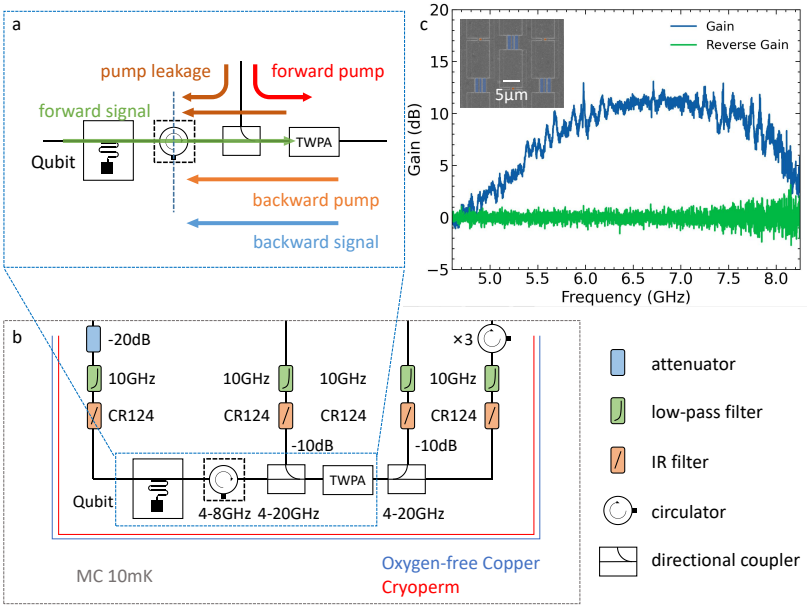


Figure 1: (a) Sketch of a typical qubit readout setup using a TWPA. Different colored arrows indicate the direction of propagation for various waves. (b) Experimental setup on the mixing chamber (MC) stage in our experiment. The frequencies of the resonator and the qubit are 7.1644 GHz and 4.87 GHz respectively. A circulator in a dasher box indicates that it was present during the first cooldown and removed during the second cooldown. (c) Forward and backward gain of the TWPA at the operating point with pump frequency $\omega_{\mathrm{p,op}}/2\pi = 6.713\,\mathrm{GHz}$ and pump power approximately $P_{\mathrm{p,op}} = -70\,\mathrm{dBm}$. (inset) A scanning electron microscopy (SEM) image which contains 3 cells of the TWPA with false coloring to indicate large (blue) and small (orange) junctions forming SNAILs.

frequency of the readout resonator and power is high, quasiparticle injection can also occur. When the pump frequency is detuned from the readout resonator, ac-Stark effect happens. Moreover, the pump power can have a range of 0.1-10 nW, depending on the level of nonlinearity. Despite the fact that the thermal power generated by the pump is significantly lower than the cooling power of the refrigerator, the qubit chip and its wiring are not well thermal anchored, and the generated heat will deposit on it, causing a series of thermal effects.

Finally, backward noise refers to the noise that propagate backward through the TWPA and then reach the qubit. The low-frequency component of this noise causes dephasing. This noise may originate from noise injected into the output port of the TWPA, or from the interaction between reflected waves and the TWPA that acts like a lossy transmission line[34]. Backward noise can become more of a problem when strong pump causes augmentation of dielectric loss, or when specific pump renders backward gain notable. The modeling and characterization of the backward noise is an open question and we do not intend to delve into it in this work. We make the assumption that the reflected noise is small and ignore it for the sake of convenience of the discussion.

It is also worth mentioning that although flux noise remains a significant source of dephasing for tunable qubits, we exclude it from our analysis. This choice is motivated by the fact that by employing appropriate magnetic shielding, flux noise from the TWPA can be effectively suppressed. Consequently, in our experiment, we utilize fixed-frequency qubits to ensure that this factor does not interfere with our observations.

### *2.4. Measurement efficiency and readout modes*

During qubit measurement, information is extracted while dephasing is induced. The efficiency of the measurement is quantified by the measurement efficiency[35], which reflects the trade-off between sensitivity and decoherence[36]. Measurement efficiency is the ratio of measurement rate to dephasing rate. That is, when dephasing is entirely caused by the intrinsic uncertainty relations through extracting information, the measurement efficiency is one. A lower measurement efficiency indicates excess dephasing beyond the inherent uncertainty. It can be measured using the method in [35], and we describe a modified version as follows:

1. Insert the measurement microwave pulse with varying amplitude $\epsilon$ and fixed duration $t_R$ between Ramsey pulses and fit the measured qubit

population $\rho_{01}$. The parameter $\tilde{\sigma}$ can be extracted by fitting $\rho_{01}(\epsilon) = \rho_{01}(0)\exp(-\epsilon^2/(2\tilde{\sigma}^2))$;
2. Measure the SNR by applying measurement pulses with varying amplitude $\epsilon$. The parameter $\tilde{a}$ can be extracted by fitting $\mathrm{SNR}(\epsilon) = \tilde{a}\epsilon$;
3. the resulting pair of parameters $\tilde{\eta} = (\tilde{\sigma}, \tilde{a})$ provides a metric for the measurement efficiency.

Note that for simplification in our experiment, we do not first calibrate an optimal integration function and an active photon depletion pulse. Instead, we use the simple weight-1 integration and soft rectangular pulse. Therefore, the SNR and $\rho_{01}$ here provide a lower bound compared to those in [35]. The value $\tilde{\sigma}^2\tilde{a}^2/2$ is not quantitatively equivalent to actual measurement efficiency $\eta$. However, to qualitatively compare different working modes, the metric $\tilde{\eta}$ can still be useful.

When the TWPA pump is involved, we define it as a separate pulse from the qubit measurement pulse. Thus we do not insert the pump with varying amplitude in the above process. Instead, we define three readout modes:

1. *off mode*: pump is always off,
2. *continuous mode*: pump is always on,
3. *pulse mode*: pump is only on during qubit measurement, and off during qubit operations.

With pulse mode, a compelling conjecture arises: qubit dephasing during qubit operation is comparable to that of off mode, as the dephasing sources we explored are significant only when the pump is on; meanwhile, the SNR during qubit measurement approaches that of continuous mode. We may thus achieve optimized measurement efficiency. This conjecture will be substantiated experimentally in the following section.

## 3. RESULTS AND DISCUSSION

In this section, we first characterize TWPA performance, and then explore the dephasing sources. Finally, we compare pulse mode with traditional modes of readout.

### *3.1. Operating point*

Our home-made TWPA consists of a long array of unit cells, each containing a Superconducting Nonlinear Asymmetric Inductive eLement (SNAIL)[37,

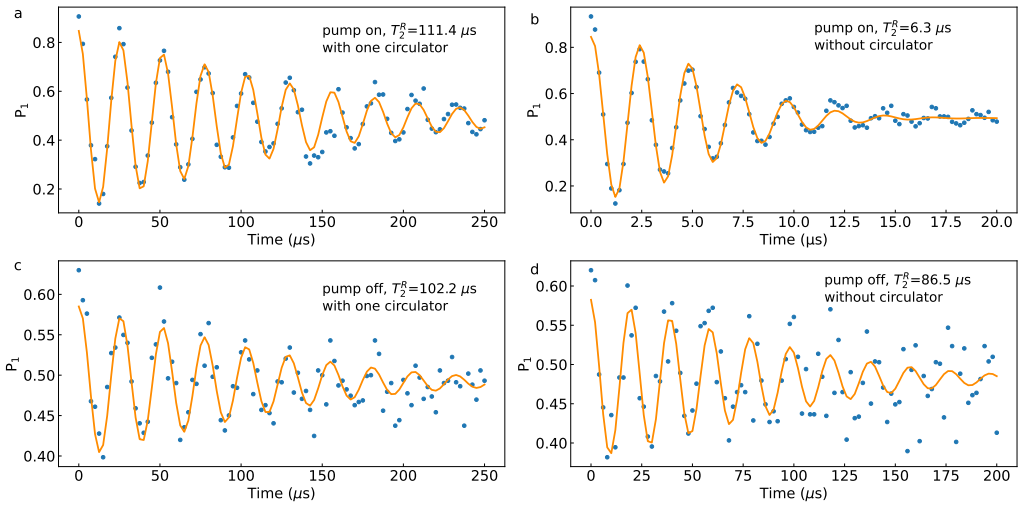


Figure 2: Ramsey fringe and fitted $T_2^{\mathrm{R}}$ with four different conditions.

31] and a pair of grounded parallel-plate capacitors. Two pads terminate the array, serving as input and output ports. Figure 3(c) (inset) is a SEM image which contains 3 out of 700 cells of our TWPA device.

Figure 1(c) shows the forward and backward gain of our TWPA at the optimal operating point, where $\omega_{\mathrm{p,op}}/2\pi = 6.713\,\mathrm{GHz}$ and pump power is around $-70\,\mathrm{dBm}$ at the input of TWPA (with $\pm 5\,\mathrm{dB}$ uncertainty from the difference of room and cryogenic temperature attenuation of CR124). Due to the critical current ratio of the small and large Josephson junctions being about 0.054, our TWPA does not exhibit the property of phase matching by adjusting external magnetic flux of SNAIL. Therefore, our TWPA actually operates at external magnetic flux $\Phi_{ext} = 0$. Backward amplification is negligible across the measurable frequency range, so it can be ignored. We characterize the forward and backward gain over a wider range of pump frequencies and powers in Supplementary Materials Sec. 2.

During the first cooldown, a circulator was present and only the first directional coupler was used. For the second cooldown, the circulator was removed and a second directional coupler added to measure backward gain. Fortunately, the TWPA operating point remains nearly unchanged, allowing direct comparison of dephasing between the cooldowns.

We measure off-resonant Ramsey fringes of the qubit with the pump on and off (Figure 2). With the pump off, $T_2^{\mathrm{R}}$ decreases slightly without the

circulator but within normal fluctuations. More important is what happens when the pump is turned on at the operating point compared to when the pump is off. With the circulator, the dephasing shows no degradation. But without it, $T_2^{\mathrm{R}}$ drops by nearly an order of magnitude, definitively showing that the pump severely impacts qubit dephasing without proper isolation. Although a circulator can provide such isolation, its insertion loss, stray magnetic fields, and bulky size are undesirable. Therefore, it is important to understand the effects of leaked pump photons on the qubit chip. In the following, we look beyond the operating point for a more general picture.

### *3.2. contribution of dephasing sources*

Let us first estimate the influence of signal reflection and backward amplification. If we assume the TWPA has a reflection coefficient $\Gamma$ around 0.1 (i.e. a characteristic impedance of 10% off from the 50 $\Omega$ environment) and take an average forward gain of 10 dB, then the backward gain from reflected pump and signal is 0.0017 dB. As to the backward gain from forward pump and reflected signal, phase matching condition is hard to achieve. Compared to exponential forward gain as a function of cell numbers in the array, this backward gain is quadratic. Assuming a moderate dispersion $\Delta k = 0.015$ and cell number of 700, we can calculate the quadratic gain to be 0.077 dB. Both backward gain from forward pump and from reflected pump are negligible, in concordance with experimental backward gain. However, the reflected signal that traverses a full cycle in TWPA back to the input port is around 10% of the original input signal, because of the forward amplification. This reflected signal is related to measurement-induced dephasing. It is equivalent to pump leakage, with a pump frequency close to qubit readout resonator. The ramifications arising from such pump leakage will be delineated subsequently.

To characterize measurement-induced dephasing, we measure the Ramsey oscillation in the presence of a continuous pump. We fix a high pump power and sweep the pump frequency around the dressed frequency of the readout resonator, which is $f_{\mathrm{r}} = 7.1644\,\mathrm{GHz}$. Note that the bare frequency of the resonator is $f_{\mathrm{r,bare}} = 7.1636\,\mathrm{GHz}$, within the scan range. Nevertheless, we can establish the range of frequencies that is affected by quasiparticle injection (marked by a shaded region) through simulation[24]. We selectively gather data beyond this realm, as the pump power remains below the threshold for quasiparticle injection. With quasiparticles disregarded, our attention shifts towards measurement-induced dephasing.

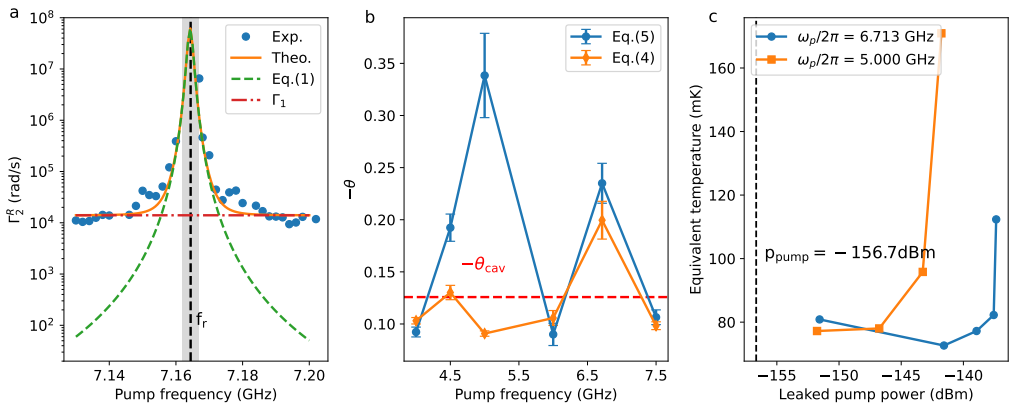


Figure 3: (a) Ramsey dephasing rate $\Gamma_2^R$ as a function of pump frequency near the readout resonator frequency (black dashed). The theoretical dephasing rate (orange solid line) is the sum of Eq.(1) (green dashed line) and a fixed $\Gamma_1$ (red dash-dot line). Their consistency supports measurement-induced dephasing as the primary cause of additional dephasing when pump frequency approaches resonator frequency. The gray area around resonator frequency demarcates the zone impacted by quasiparticle injection and we do not collect data there. (b) Extracted $\theta$ from qubit dephasing rate (orange) and dressed frequency (blue) for pump frequencies detuned from the readout resonator frequency. $\theta_{\text{cav}}$ (red dashed) is calculated from the fitted $\kappa$ in (a). The consistency exhibited by the three curves indicates that ac-Stark effect is the main source of qubit dephasing when pump frequency is off-resonant to readout resonator. (c) Qubit equivalent temperature as a function of pump power at two different pump frequencies: the frequency of the operating point (blue) and near qubit frequency (orange). The black dashed line indicates the leaked pump power at the operating point. Leaked pump may causes thermal population of the qubit, but only at a power much higher than our operating point.

We fit $f_{\mathrm{q}}$ and $\Gamma_2^{\mathrm{R}}$ from the Ramsey oscillation simultaneously using Eqs.(1) to (3). The fitted $\kappa/2\pi = 2.17\,\mathrm{MHz}$ exceeds the $\kappa/2\pi = 0.784\,\mathrm{MHz}$ measured with qubit ac Stark shift, possibly because of the accelerated resonator decay from the high pump power. The fitted $\Gamma_1/2\pi = 2.99\,\mathrm{kHz}$ agrees with the $T_1$ measured from the standard method. It remains constant with pump frequency, showing that $T_1$ is unaffected by the pump.

The theoretical pure dephasing from Eq.(1) and total dephasing $\Gamma_{2\mathrm{R}}$ with the fitted parameters are plotted in Figure 3(a) along with the experimental data. Their consistency supports measurement-induced dephasing as the primary cause of additional dephasing when pump frequency approaches resonator frequency. The dephasing rate increases rapidly when the pump frequency approaches $f_{\mathrm{r}}$; thus it is best to avoid choosing pump frequency near any readout resonator. The fitted qubit frequency is plotted in Supplementary Materials Figure S1.

Next, we conduct a similar measurement but sweep the pump power across a range of pump frequencies to investigate the ac-Stark effect. $\theta$ can be extracted from qubit dephasing rate through Eq.(4) or from dressed frequency through Eq.(5). Figure 3(b) displays the $\theta$ values and their standard errors obtained using both methods. The consistency between the two sets of values indicates that our ac-Stark model can accurately represent the dephasing induced by the off-resonant pump. Also, we calculate a $\theta_{\mathrm{cav}}$ from the fitted value of $\kappa$ from Figure 3(a), and find it close to the above fitted $\theta$ values. This finding indicates that the ac-Stark effect may share the same origin as measurement-induced dephasing. The remaining discrepancy could be because $\theta$ is not negligible enough for our approximation to be accurate.

We proceed with measuring the thermal population of the qubit as an indicator of thermal effects, assuming that heating is the primary cause of the extra thermal population in the qubit, provided that the pump does not directly excite the qubit. To estimate the thermal population, we use the contrast of $|e\rangle$-$|f\rangle$ Rabi oscillation with and without a $|g\rangle$-$|e\rangle$ $\pi$ pulse. The equivalent temperature of the qubit can then be calculated (Figure 3(c)), assuming a Maxwell-Boltzmann distribution between $|g\rangle$ and $|e\rangle$, with the negligible population on higher energy levels[38]. The pump powers are calculated from the linear fit of attenuation used in Figure 3(b) (see Section 5). We note that this leaked pump power is the power that directly dresses the qubit, and constitutes only a fraction of the total leaked power which contributes to heating. We observe that the temperature climbs rapidly with pump power when the power is high, despite the pump being off-resonant

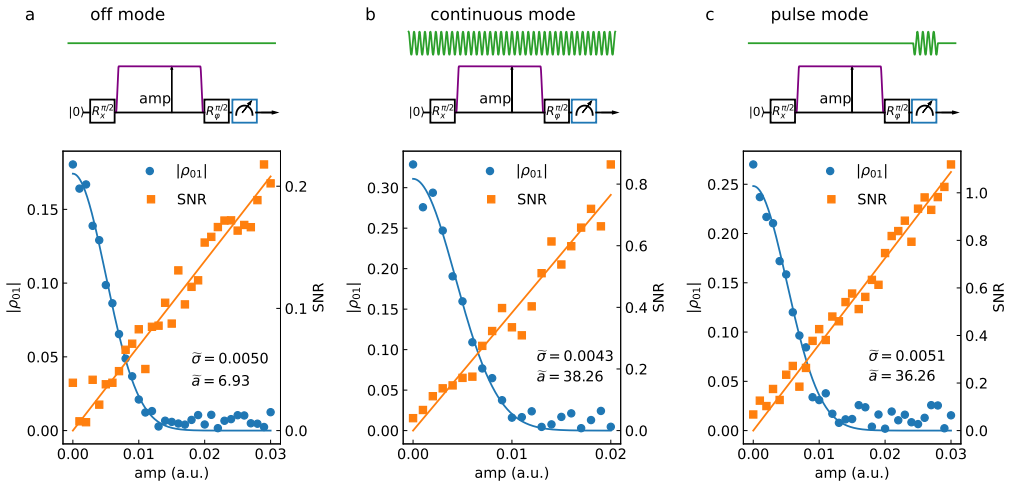


Figure 4: Extraction of modified measurement efficiency with (a) off mode (b) continuous mode and (c) pulse mode.

with respect to the readout resonator. Additionally, for the pump frequency with a small detuning from the qubit frequency ($f_q = 4.87\,\mathrm{GHz}$), the temperatures are higher than those observed at the pump frequency of the operating point.

Regarding pump leakage, the primary cause for the drop in dephasing time in Figure 2 is the ac Stark effect. At the working point, the pump frequency is sufficiently far from the readout resonator and the pump power (indicated as a dashed black line in Figure 3(c)) is much lower than the powers that can cause heating. As a result, this pump is incapable of inducing strong measurement-induced dephasing or heating.

### *3.3. Pulse mode*

Finally, we evaluate the three modes using measurement efficiency as a metric without circulator between qubit chip and TWPA, as discussed in Section 2.4. While we do not quantitatively measure the measurement efficiency, we can still compare the modes based on the extracted values of $\tilde{\eta} = (\tilde{\sigma}, \tilde{a})$. We observe that off mode and pulse mode have similar values of $\tilde{\sigma}$, while continuous mode has a smaller one. This suggests that pulse mode can mitigate the dephasing caused by continuous pumping during operations. Meanwhile, $\tilde{a}$ is much higher in pulsed and continuous modes than in off

mode. Although $\tilde{a}$ in pulse mode is slightly smaller than in continuous mode, this is mainly due to the lack of calibration of the timing between pump and measurement pulses and can be easily compensated. The crucial advantage of pulse mode is that it achieves both high SNR and low backaction to the system during operation, which agrees with our conjecture.

The measurement efficiency of a TWPA is limited by several factors and can be further improved through a combination of design, material, fabrication, and control efforts. Firstly, a TWPA contains numerous sidebands that extract quantum information from the signal but are never detected. A clever design can avoid such leakage [39]. Secondly, insertion loss cannot be ignored as the ground plane is made of gold and the substrate is also lossy. The use of better materials may decrease such loss. Thirdly, there is a reflection of signal due to fluctuations in junction parameters which can be improved through fabrication optimization for more stable and uniform junction resistances. Last but not least, strategies such as optimizing the timing between measurement and pump pulses and employing pulse shaping techniques like Cavity Level Excitation and Reset (CLEAR) pulse[40] can also help push measurement efficiency limits.

## 4. CONCLUSIONS

We theoretically and experimentally explore the potential sources of dephasing of a qubit connected to a TWPA for readout. Among these sources, pump leakage is important, causing measurement-induced dephasing, ac-Stark shifts, and heating. While we do not conceive the pulse mode itself, we have exhibited its inherent value in enhancing the SNR of readout with minimal compromise to dephasing. Pulse-mode readout is ideal for one-time readout applications, but can also benefit applications alternating measurements and operations. However, dephasing can only be partially mitigated in these cases. Furthermore, the dephasing mechanisms discussed here can help determine the optimal operation points in all applications that use microwave-pumped preamplifiers like JPAs and TWPAs. For instance, it is important to avoid placing the qubit idling point, resonator frequency, and pump frequency too close to each other, even with circulators for isolation.

The combination of pulse mode and circulators shows promise as an approach to accommodate microwave-pumped preamplifiers in fault-tolerant quantum computing architectures[41]. Achieving fast and high-efficiency simultaneous readout of large qubit arrays is pivotal for translating quantum

error correction from theory to reality. Our work illuminates a way to overcome this formidable challenge by mitigating the deleterious pump-induced dephasing effects. With continued progress in understanding and optimizing the interface between qubits and microwave-pumped amplifiers at a fundamental level, the high-quality readout required for fault tolerance may become achievable.

## 5. METHODS

### *5.1. Measurement setup*

As shown in Figure 1(b), our qubit chip utilizes a readout resonator that couples to a transmission line to perform dispersive readout. A circulator is selectively added between the qubit chip and a directional coupler. This directional coupler feeds the TWPA by combining qubit readout signal and a pump. Note that the directional coupler has a higher impedance mismatch to the TWPA than a circulator, so we place it as close to the TWPA as possible to avoid standing waves. To measure backward gain, the output port of the TWPA has another directional coupler for the backward pump, and all input and output channels are filtered with low-pass and infrared filters. Additionally, we use three circulators to block noise from the HEMT. Finally, the Cryoperm shielding effectively isolates the system from magnetic noise. Our experimental setup is compatible with the typical setup discussed in Section 2.3, with the additional directional coupler acting as a lossy wire.

### *5.2. Fitting*

For Figure 3(a), We fit $f_{\mathrm{q}}$ and $\Gamma_2^{\mathrm{R}}$ from the Ramsey oscillation at each pump frequency. From the acquired data, we simultaneously fit $f_{\mathrm{q}}$ and $\Gamma_2^{\mathrm{R}}$ as a function of $f_{\mathrm{p}}$ to Eqs.(2) and (1) with three parameters: $\kappa$, $\epsilon_p$ and $\Gamma_1$. The parameter $\chi/2\pi = -0.137\,\mathrm{MHz}$ is calibrated in advance. We obtain the fitted parameters $\kappa/2\pi = 2.17\,\mathrm{MHz}$ and $\Gamma_1/2\pi = 2.99\,\mathrm{kHz}$.

For Figure 3(b), We assume $T_1 = 129\,\mu\mathrm{s}$ remains constant with varying pump parameters and use it to calculate $\Gamma_\phi$ from $\Gamma_2^{\mathrm{R}}$. As the pump power leaked to and sensed by the qubit is unknown, we make the assumption that the attenuation en route in dB is linearly dependent on frequency and obtain a reasonable fit to the experimental data. From Eq.(4) and Eq.(5), we can see $\Gamma_{\phi,ac}$ and $\Delta\omega_q$ are linear to this leaked pump power. By employing the same linear function of attenuation with frequency as a fitting model, we

obtain distinct values for $\theta$ corresponding to varying pump power utilizing two different formulas Eq.(4) and Eq.(5).

## References


[1] Mutus, J. Y. et al. Strong environmental coupling in a Josephson parametric amplifier. *Appl. Phys. Lett.* 104, 263513 (2014). doi: https://doi.org/10.1063/1.4886408.

[2] Bockstiegel, C. et al. Development of a Broadband NbTiN Traveling Wave Parametric Amplifier for MKID Readout. *J. Low Temp. Phys.* 176, 476 (2014). doi:10.1007/s10909-013-1042-z.

[3] Macklin, C. et al. A near–quantum-limited Josephson traveling-wave parametric amplifier. *Science* 350, 307 (2015). doi: https://link.aps.org/doi/10.1126/science.aaa8525.

[4] White, T. C. et al. Traveling wave parametric amplifier with Josephson junctions using minimal resonator phase matching. *Appl. Phys. Lett.* 106, 242601 (2015). doi:https://doi.org/10.1063/1.4922348.

[5] Vissers, M. R. et al. Low-noise kinetic inductance traveling-wave amplifier using three-wave mixing. *Applied Physics Letters* 108, 012601 (2016). doi:10.1063/1.4937922.

[6] Planat, L. et al. Photonic-crystal Josephson traveling-wave parametric amplifier. *Phys. Rev. X* 10, 021021 (2020). doi: https://doi.org/10.1103/PhysRevX.10.021021.

[7] Malnou, M. et al. Three-wave mixing kinetic inductance traveling-wave amplifier with near-quantum-limited noise performance. *PRX Quantum* 2, 010302 (2021). doi:10.1103/PRXQuantum.2.010302.

[8] Córcoles, A. D. et al. Exploiting dynamic quantum circuits in a quantum algorithm with superconducting qubits. *Phys. Rev. Lett.* 127, 100501 (2021). doi:https://doi.org/10.1103/PhysRevLett.127.100501.

[9] Acharya, R. et al. Suppressing quantum errors by scaling a surface code logical qubit. *Nature* 614, 676 (2023). doi: https://doi.org/10.1038/s41586-022-05434-1.

[10] Daley, A. J. et al. Practical quantum advantage in quantum simulation. *Nature* 607, 667 (2022). doi:https://doi.org/10.1038/s41586-022-04940-6.

[11] Lled, C. et al. Cloaking a qubit in a cavity. Preprint at https://doi.org/10.48550/arXiv.2211.05758 (2022).

[12] Eichler, C. et al. Controlling the dynamic range of a Josephson parametric amplifier. *EPJ Quantum Technology* 1, 2 (2014). doi: https://doi.org/10.1140/epjqt2.

[13] Roch, N. et al. Observation of measurement-induced entanglement and quantum trajectories of remote superconducting qubits. *Phys. Rev. Lett.* 112, 170501 (2014). doi: https://doi.org/10.1103/PhysRevLett.112.170501.

[14] Jebari, S. et al. Near-quantum-limited amplification from inelastic Cooper-pair tunnelling. *Nat. Electron.* 1, 223 (2018). doi: https://doi.org/10.1038/s41928-018-0055-7.

[15] Sliwa, K. M. et al. Reconfigurable Josephson circulator/directional amplifier. *Phys. Rev. X* 5, 041020 (2015). doi: https://doi.org/10.1103/PhysRevX.5.041020.

[16] Rosenthal, E. I. et al. Efficient and low-backaction quantum measurement using a chip-scale detector. *Phys. Rev. Lett.* 126, 090503 (2021). doi:https://doi.org/10.1103/PhysRevLett.126.090503.

[17] Wang, C. et al. Towards practical quantum computers: transmon qubit with a lifetime approaching 0.5 milliseconds. *NPJ Quantum Inf.* 8, 3 (2022). doi:https://doi.org/10.1038/s41534-021-00510-2.

[18] Gambetta, J. et al. Qubit-photon interactions in a cavity: Measurement-induced dephasing and number splitting. *Phys. Rev. A* 74, 042318 (2006). doi:https://doi.org/10.1103/PhysRevA.74.042318.

[19] Sears, A. P. et al. Photon shot noise dephasing in the strong-dispersive limit of circuit QED. *Phys. Rev. B* 86, 180504 (2012). doi: https://doi.org/10.1103/PhysRevB.86.180504.

[20] Clerk, A. A. et al. Using a qubit to measure photon-number statistics of a driven thermal oscillator. *Phys. Rev. A* 75, 042302 (2007). doi: https://doi.org/10.1103/PhysRevA.75.042302.

[21] Goetz, J. et al. Photon statistics of propagating thermal microwaves. *Phys. Rev. Lett.* 118, 103602 (2017). doi: https://link.aps.org/doi/10.1103/PhysRevLett.118.103602.

[22] Bertet, P. et al. Dephasing of a superconducting qubit induced by photon noise. *Phys. Rev. Lett.* 95, 257002 (2005). doi: https://link.aps.org/doi/10.1103/PhysRevLett.95.257002.

[23] Wang, Z. et al. Cavity attenuators for superconducting qubits. *Phys. Rev. Appl.* 11, 014031 (2019). doi: https://link.aps.org/doi/10.1103/PhysRevApplied.11.014031.

[24] Wang, C. et al. Measurement and control of quasiparticle dynamics in a superconducting qubit. *Nature Comm.* 5, 5836 (2014). doi: https://doi.org/10.1038/ncomms6836.

[25] Wei, K. X. et al. Hamiltonian engineering with multicolor drives for fast entangling gates and quantum crosstalk cancellation. *Phys. Rev. Lett.* 129, 060501 (2022). doi: https://link.aps.org/doi/10.1103/PhysRevLett.129.060501.

[26] Zhao, P. et al. Combating fluctuations in relaxation times of fixed-frequency transmon qubits with microwave-dressed states. *Phys. Rev. A* 105, 062605 (2022). doi:https://doi.org/10.1103/PhysRevA.105.062605.

[27] Van Harlingen, D. J. et al. Decoherence in Josephson-junction qubits due to critical-current fluctuations. *Phys. Rev. B* 70, 064517 (2004). doi:https://doi.org/10.1103/PhysRevB.70.064517.

[28] Caves, C. M. Quantum limits on noise in linear amplifiers. *Phys. Rev. D* 26, 1817 (1982). doi:10.1103/PhysRevD.26.1817.

[29] Houde, M. et al. Loss asymmetries in quantum traveling-wave parametric amplifiers. *Phys. Rev. Appl.* 12, 034054 (2019). doi: 10.1103/PhysRevApplied.12.034054.

[30] Yuan, Y. et al. Circuit quantum electrodynamic model of dissipative-dispersive Josephson traveling-wave parametric amplifiers. *Phys. Rev. A* 107, 022612 (2023). doi:https://doi.org/10.1103/PhysRevA.107.022612.

[31] Ranadive, A. et al. Kerr reversal in Josephson meta-material and traveling wave parametric amplification. *Nature Comm.* 13, 1737 (2022). doi:https://doi.org/10.1038/s41467-022-29375-5.

[32] O'Brien, K. et al. Resonant phase matching of Josephson junction traveling wave parametric amplifiers. *Phys. Rev. Lett.* 113, 157001 (2014). doi:https://link.aps.org/doi/10.1103/PhysRevLett.113.157001.

[33] Zhao, S. et al. Quantum analysis of second-order effects in superconducting travelling-wave parametric amplifiers. *J. Phys. D* 54, 365303 (2021). doi:https://doi.org/10.1088/1361-6463/ac0b74.

[34] Zurita-Sánchez, J. R. et al. Lossy electrical transmission lines: Thermal fluctuations and quantization. *Phys. Rev. A* 73, 063825 (2006). doi: 10.1103/PhysRevA.73.063825.

[35] Bultink, C. C. et al. General method for extracting the quantum efficiency of dispersive qubit readout in circuit QED. *Appl. Phys. Lett.* 112, 092601 (2018). doi:https://doi.org/10.1063/1.5015954.

[36] Clerk, A. A. et al. Introduction to quantum noise, measurement, and amplification. *Rev. Mod. Phys.* 82, 1155 (2010). doi: https://link.aps.org/doi/10.1103/RevModPhys.82.1155.

[37] Frattini, N. E. et al. 3-wave mixing Josephson dipole element. *Appl. Phys. Lett.* 110, 222603 (2017). doi:https://doi.org/10.1063/1.4984142.

[38] Jin, X. Y. et al. Thermal and residual excited-state population in a 3d transmon qubit. *Phys. Rev. Lett.* 114, 240501 (2015). doi: https://doi.org/10.1103/PhysRevLett.114.240501.

[39] Peng, K. et al. Floquet-mode traveling-wave parametric amplifiers. *PRX Quantum* 3, 020306 (2022). doi: https://doi.org/10.1103/PRXQuantum.3.020306.

[40] McClure, D. T. et al. Rapid driven reset of a qubit readout resonator. *Phys. Rev. Appl.* 5, 011001 (2016). doi: https://doi.org/10.1103/PhysRevApplied.5.011001.

[41] Preskill, J. *Fault-tolerant quantum computation*, pages 213–269. doi: https://doi.org/10.1142/9789812385253_0008.

## MISCELLANEA

**funding** This work is supported by the National Natural Science Foundation of China (NSFC-11890704) and the Natural Science Foundation of Beijing (NSFB-Z190012), and the Key Area Research and Development Program of Guangdong Province (Grant No.2018B030326001).

**Declaration of Competing Interest** The authors declare no competing interests.

a

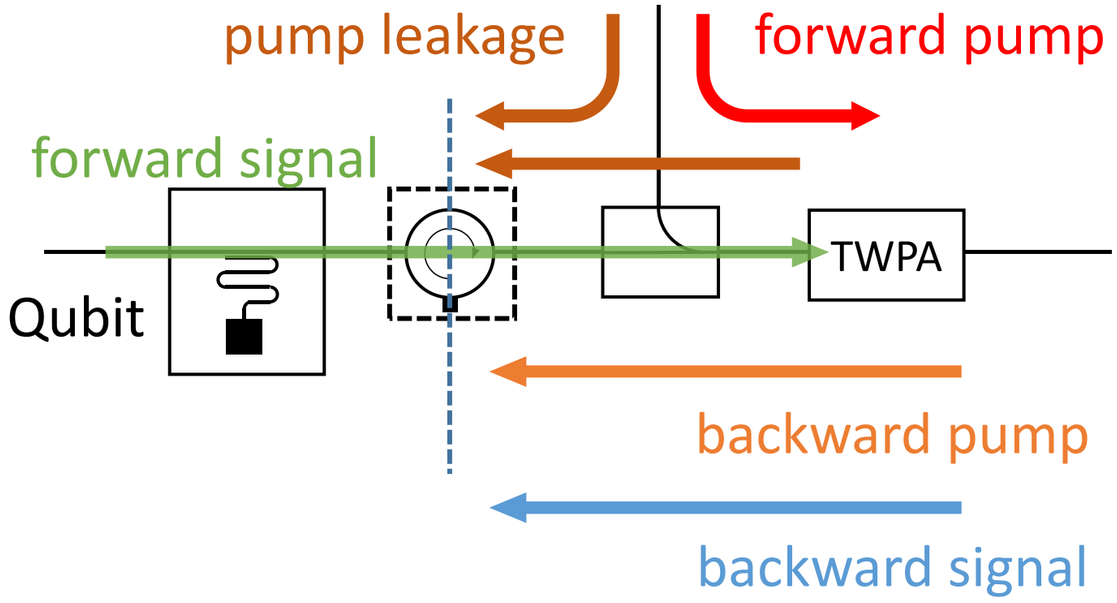


c

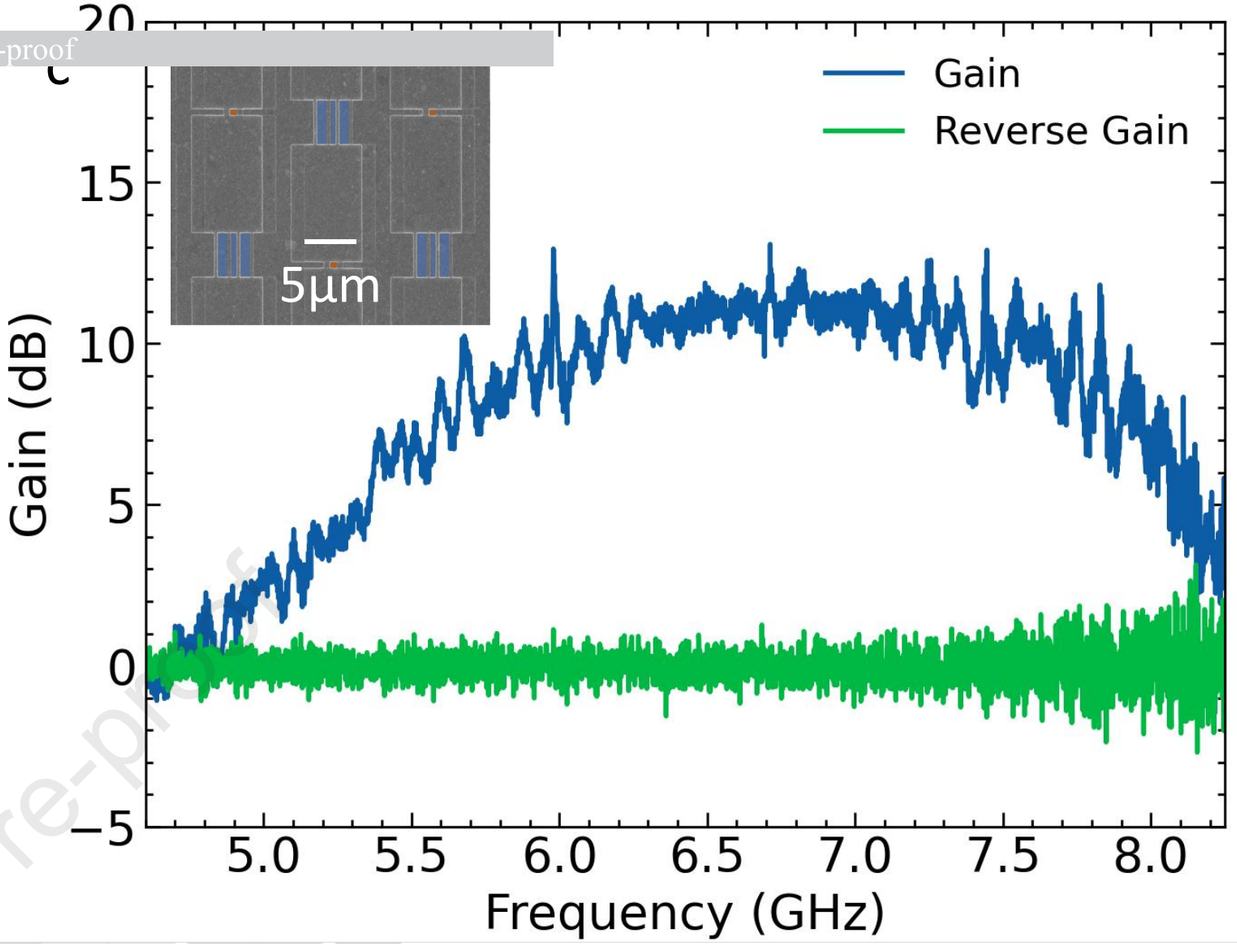


b

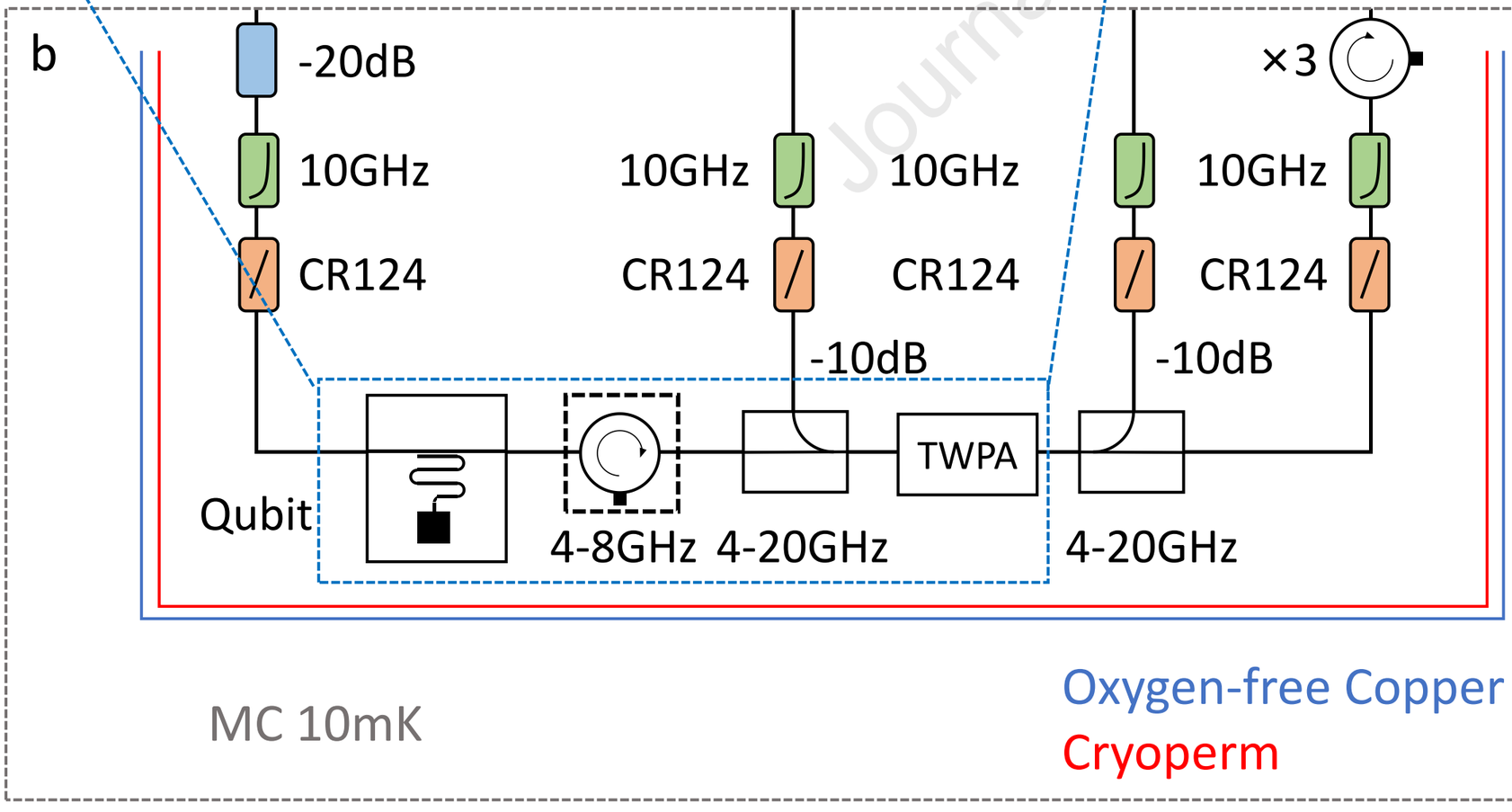


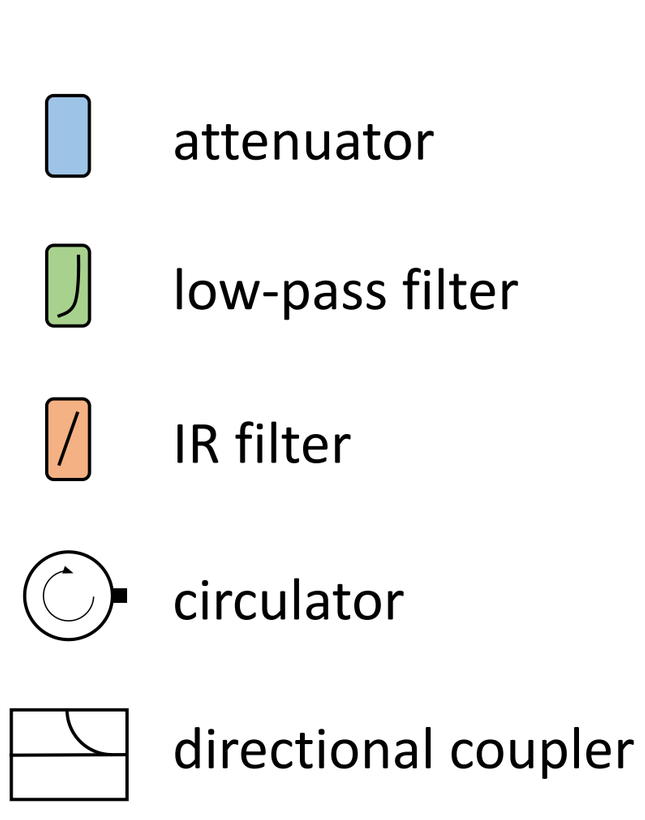

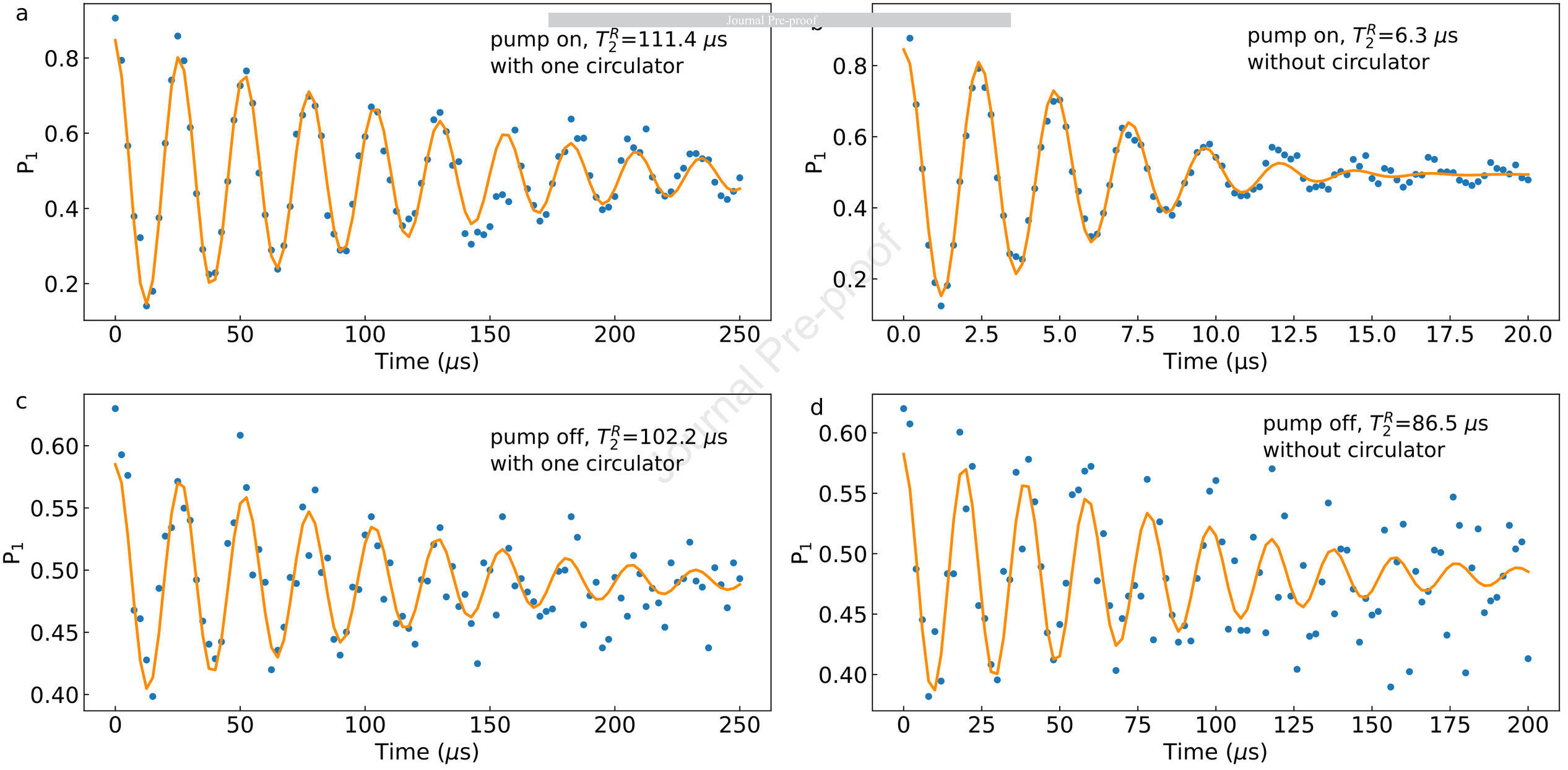

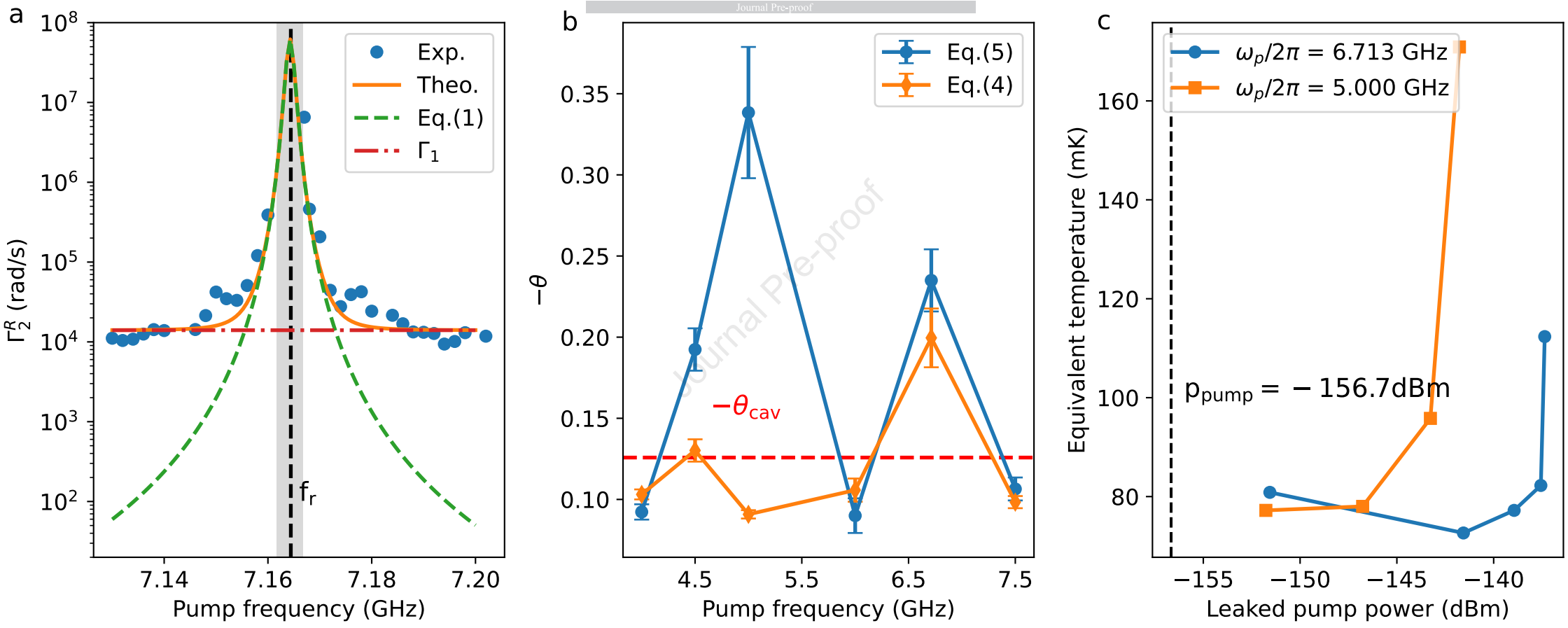
a
$10^8$
$10^7$
$10^6$
$10^5$
$10^4$
$10^3$
$10^2$
$\Gamma_2^R$ (rad/s)
Exp.
Theo.
Eq.(1)
$\Gamma_1$
$f_r$
7.14
7.16
7.18
7.20
Pump frequency (GHz)
b
Journal Pre-proof
Eq.(5)
Eq.(4)
$-\theta$
0.35
0.30
0.25
0.20
0.15
0.10
$-\theta_{cav}$
4.5
5.5
6.5
7.5
Pump frequency (GHz)
c
$\omega_p/2\pi$ = 6.713 GHz
$\omega_p/2\pi$ = 5.000 GHz
Equivalent temperature (mK)
160
140
120
100
80
$p_{pump} = -156.7$dBm
−155
−150
−145
−140
Leaked pump power (dBm)

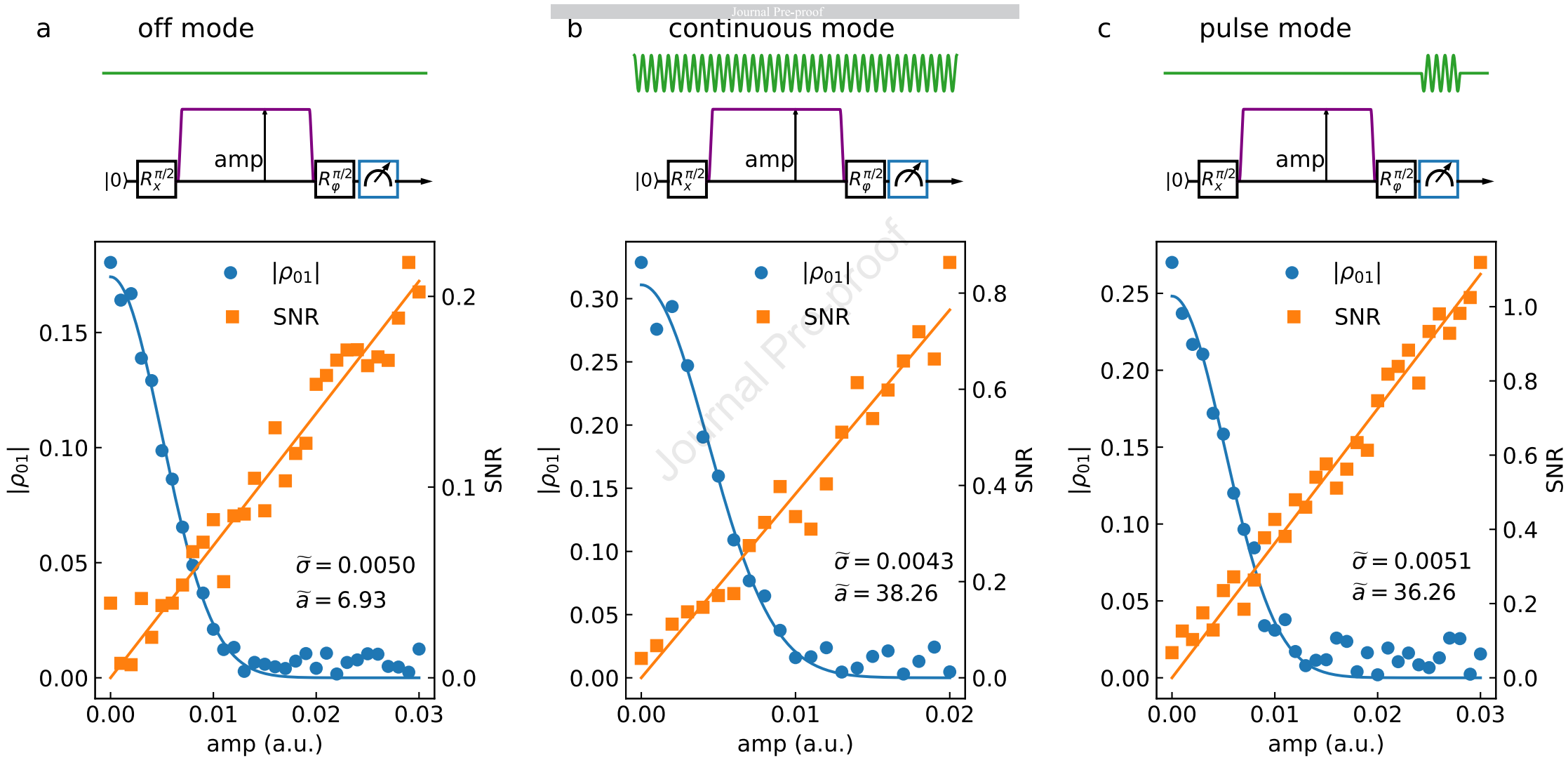

**Declaration of interests**

☒ The authors declare that they have no known competing financial interests or personal relationships that could have appeared to influence the work reported in this paper.

☒The authors declare the following financial interests/personal relationships which may be considered as potential competing interests:

| |
|---|
| None |